Defect detection in composites by three-dimensional generative principal component thermography

by F. Wang*, J. Jiang*, S. Sfarra**, Y. Yao*** and Y. Liu*

* Institute of Process Equipment and Control Engineering, Zhejiang University of Technology, Hangzhou, 310023 China, *2112102479@zjut.edu.cn, jiangzl@zjut.edu.cn, 221123020532@zjut.edu.cn, yliuzju@zjut.edu.cn*

** *Department of Industrial and Information Engineering and Economics, University of L'Aquila, Piazzale E. Pontieri no. 1, Monteluco di Roio – L'Aquila (AQ), I-67100, Italy, stefano.sfarra@univaq.it*

*** Department of Chemical Engineering, National Tsing Hua University, Hsinchu, 30013, Taiwan, *yyao@mx.nthu.edu.tw*

Abstract

Deep learning has emerged as a promising tool for the nondestructive evaluation of polymer composites. However, its data analysis capability remains fundamentally constrained by the limited availability of thermographic data. To address this challenge, we propose a novel method, three-dimensional Generative Adversarial Network Principal Component Thermography (3DGPCT), for defect detection. By employing 3D convolutional operations, it can enable the generator to capture the global spatial distribution of objects, thereby maintaining structural consistency in all directions. The generated data are subsequently fused with the original images, and discriminative features are further extracted using principal component thermography. Experimental validation on carbon fiber composite specimens containing six types of defects demonstrates the effectiveness of the proposed defect detection method.

Keywords: active pulsed infrared thermography, three-dimensional convolution, generative adversarial networks, carbon fiber reinforced polymer

1. Introduction

With the rapid growth in demand for polymer composites in aerospace, automotive, and related industries [1-3], the efficient and accurate detection of internal defects has become a central research focus in materials science. Conventional nondestructive evaluation (NDE) techniques, such as ultrasonic testing [4] and radiographic inspection [5], are widely used but suffer from several limitations, including being time-consuming, costly, and lacking sensitivity to complex structures. In recent years, non-contact NDE methods based on active pulsed thermography (APT) [6-8] have demonstrated significant potential owing to their rapidity, efficiency, and ability to provide intuitive visualizations.

In recent years, deep learning techniques [9-11] have demonstrated remarkable capabilities in data analysis and feature extraction, achieving significant breakthroughs in tasks such as image recognition [12], object detection [13], and pattern classification [14]. Within materials science, deep learning has increasingly been applied to defect detection, enabling the automatic extraction of latent features from complex data through deep neural network architectures and thereby facilitating efficient identification of internal defects. However, the successful deployment of deep learning models typically requires large volumes of high-quality training data. In practice, the acquisition of extensive thermographic datasets is often constrained by costs and experimental limitations, resulting in insufficient and suboptimal data quality. These challenges substantially hinder the widespread application of deep learning for nondestructive evaluation of polymer composites.

To address the challenge of insufficient data, generative adversarial networks (GANs) [15] have attracted considerable attention in recent years. By leveraging two adversarial networks, GANs can effectively augment both the quantity and quality of training data. In the field of APT, two-dimensional GANs (2DGANs) [16] are commonly employed to generate thermographic data based on two-dimensional images. While these approaches enhance dataset diversity, they are inherently limited to planar spatial information and thus fail to capture the complex three-dimensional structural features. This limitation becomes particularly pronounced when analyzing spatiotemporal information of APT data.

To overcome the limitations of conventional 2DGANs in capturing spatial structural features, a defect detection method based on 3D generative adversarial network principal component thermography (3DGPCT) is proposed. This approach utilizes a 3D convolutional architecture to effectively learn the spatial distribution characteristics of internal defects within materials, enabling the generation of structurally consistent and high-quality thermographic data in all orientations. Furthermore, discriminative features are extracted through principal component thermography, facilitating precise defect identification. To validate the effectiveness of the 3DGPCT method, experiments were conducted on carbon fiber reinforced polymer (CFRP) specimens containing six representative defect types. The experimental results demonstrate that the proposed approach not only alleviates the limitations imposed by insufficient data but also significantly enhances the accuracy and robustness of internal defect detection in polymer composites. Quantitative analysis based on contrast-to-noise ratio (CNR) further corroborates the efficacy of the proposed method.

2. Data Acquisition and Preprocessing

In this study, experimental data were acquired using APT. The experimental setup consisted of the CFRP specimen, two high intensity pulsed lamps, an infrared thermal camera, and a computer for data acquisition and analysis. During the experiment, the surface of the specimen was subjected to transient heating using the pulsed light sources, resulting in a swift temperature increase. The infrared thermal camera then continuously captured a time series of thermographic images at a high frame rate, recording the temporal evolution of the specimen surface temperature. The presence of internal microstructural anomalies or damage, which possess thermal properties distinct from the surrounding materials, leads to localized variations in heat conduction. These differences manifest as pronounced temperature changes in the thermal image sequence, enabling direct observation and recording of dynamic thermal distributions for subsequent defect identification.

The raw thermal image data were structured as a three-dimensional matrix of size $n \times h \times w$, where n is the number of frames, and h and w denote the height and width of each image, respectively. After extraction, the data were reshaped into a two-dimensional matrix of $n \times t$ (where t is the number of pixels per frame), with each row representing a thermal image frame and each column corresponding to the temperature trajectory of a specific pixel over time. To ensure data comparability across different samples and to enhance model training efficiency, Min-Max normalization was applied to each row, scaling pixel temperature values linearly to the range [0, 1]. This normalization guaranteed consistent dimensionality and value range for all input data, thereby facilitating subsequent deep learning model analysis.

3. Methodology

3.1. Basic Knowledge

The Generative Adversarial Network (GAN) is a deep learning framework grounded in game theory and comprises two main components: a generator and a discriminator. The core principle of GANs is to enable the generator (G) to learn the distribution of real data through adversarial training against the discriminator (D). The generator takes a random noise vector z as input and produces synthetic samples $G(z)$, while the discriminator receives input samples x and outputs the probability $D(x)$ that the sample is real. The objective function of GANs is defined as follows:

$$\min_G \max_D V\left(D,G\right) = \mathrm{E}_{x\sim p_{data(x)}}\left[\log D\left(x\right)\right] + \mathrm{E}_{z\sim p_{z(z)}}\left[\log\left(1-D\left(G\left(z\right)\right)\right)\right] \tag{1}$$

here, $p_{data(x)}$ denotes the distribution of real data, and $p_{z(z)}$ represents the noise distribution. $E_{x\sim pdata(x)}$ and $E_{z\sim pz(z)}$ correspond to the expectations over the real data and noise distributions, respectively. During training, G and D are alternately optimized with respect to their own objectives, ultimately leading to a generator that produces samples indistinguishable from real data by the discriminator.

The two-dimensional generative adversarial network (2DGAN) is an adaptation of GANs for two-dimensional image applications and is widely utilized in scenarios such as infrared thermography. Typically, both the G and D in 2DGAN are constructed based on convolutional neural networks (CNNs), allowing for effective extraction and utilization of spatial features within images. The generator takes a noise vector z as input and outputs a two-dimensional image $G(z)$, while the discriminator determines whether a given 2D image is real or generated. The training loss function of 2DGAN closely resembles that of the classical GAN framework. 2DGANs have shown excellent performance in tasks such as thermographic image enhancement and defect detection; however, their capacity for modeling complex three-dimensional structures is limited. Consequently, for applications requiring preservation of spatial consistency, three-dimensional generative adversarial network (3DGAN) represents a promising direction for further advancement in the field of APT.

3.2. 3DGPCT

The 3DGAN is a GAN architecture that employs three-dimensional convolutional neural networks as its core structure. Both the G and D are implemented using 3D convolutional layers, enabling the model to capture complex relationships in both the spatial and temporal dimensions of infrared thermographic sequences. This enhances the network's ability to detect subtle defects and recognize spatial distribution characteristics. In applications such as APT, the acquired thermal image sequences typically consist of multiple time frames and are structured as three-dimensional data cubes. The specific framework of 3DGPCT is illustrated in Figure 1.

Similar to 2DGANs, the G in 3DGAN takes a low-dimensional random noise vector z as input and utilizes multiple layers of three-dimensional deconvolution to map the noise into a three-dimensional sample that closely resembles real infrared thermographic 3D data. The specific process is as follows:

$$\hat{x} = G\left(z,\theta_g\right) \tag{2}$$

where $\hat{x}$ denotes the generated 3D thermographic data, and θ_g represents the parameters of the *G* network. The objective of the *G* is to maximize the probability that the *D* incorrectly classifies the generated samples as real. By continuously optimizing its parameters, the *G* learns the spatial distribution characteristics of infrared thermographic data, thereby enabling effective simulation of complex spatial structures and temperature gradients.

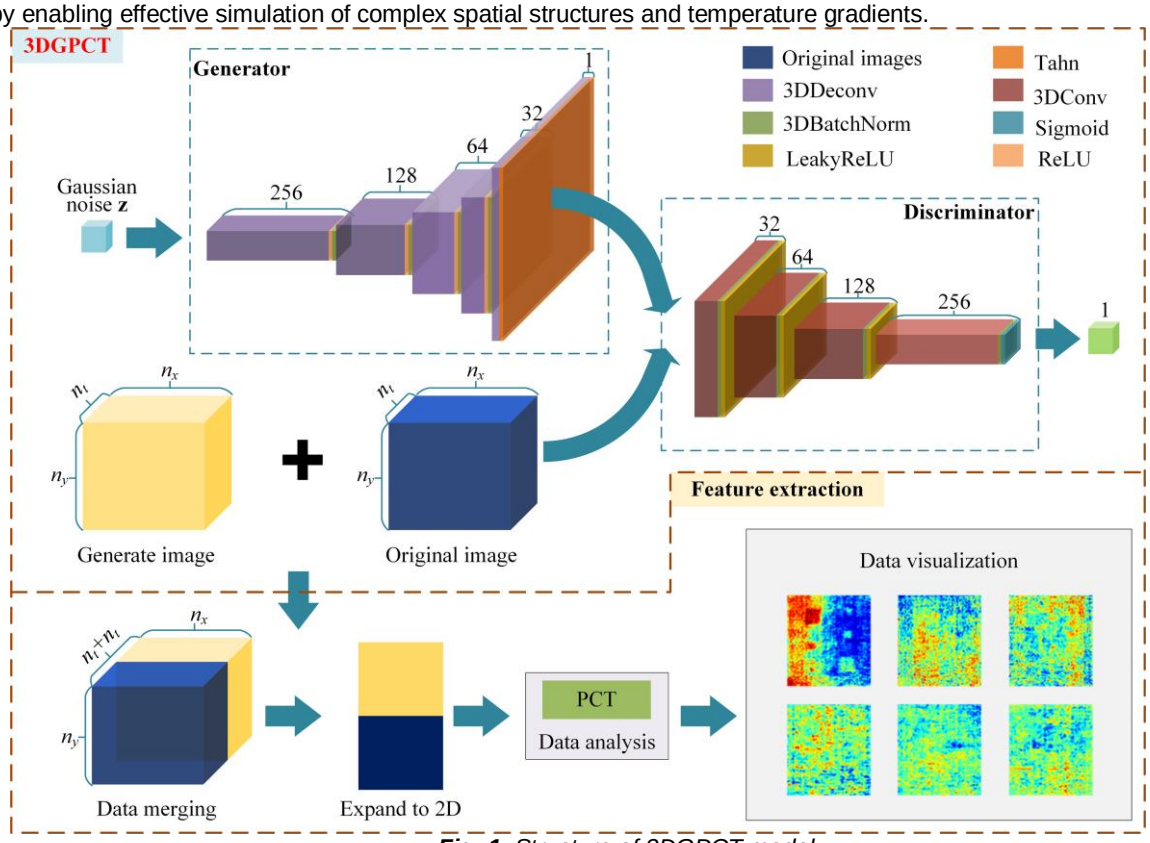

Fig. 1. *Structure of 3DGPCT model*

The *D*, as a key component of the adversarial training framework, is tasked with distinguishing whether the input three-dimensional data are authentic infrared thermographic volumes or synthetic samples produced by *G*. *D* typically adopts a multi-layer three-dimensional convolutional neural network structure, which allows it to thoroughly extract high-order spatial features from the data. By receiving input three-dimensional thermographic data, *D* learns to recognize the distributional differences between real and generated samples, ultimately outputting a probability value that reflects the authenticity of the input sample:

$$D\left(\bar{x};\theta_d\right)\rightarrow\left[0,1\right] \tag{3}$$

where, $\bar{x}$ denotes the generated three-dimensional thermographic data, θ_d represents the generator parameters, and *D*(·) outputs a scalar value indicating the probability that the input sample is real. During adversarial training, the *D* continuously improves its ability to distinguish between genuine and synthetic three-dimensional thermographic data, thereby compelling the *G* to produce samples that increasingly resemble the real data distribution. Notably, 3DGAN adopts an objective function similar to that of conventional GANs. Through adversarial training, 3DGAN can generate highly structured and temporally consistent three-dimensional thermographic data. By merging the generated data with the original images, this approach addresses the issue of limited data diversity in the original dataset.

Initially, column normalization is applied to preprocess the thermographic images. By effectively scaling each column of data according to its feature range, the relative importance of different features is balanced. This process significantly enhances data quality and prepares the dataset for subsequent model input. To further facilitate optimal network training, the thermographic data are resized to match the appropriate network input dimensions, ensuring that the original thermographic information is preserved for the deep learning model.

Subsequently, the pre-processed thermographic data are input into the 3DGPCT model. The final architecture for both the *G* and *D* consists of five layers each. Except for the first 3D transposed convolution in G and the last 3D convolution in *D*, which use 0 padding, all other layers employ a kernel size of 4, a stride of 1, and a padding of 1. Three-dimensional batch normalization is applied after each layer to accelerate training and enhance stability.

During the training of 3DGAN, the *G* receives a low-dimensional random noise vector as input. In each training iteration, the noise is mapped through multiple layers of 3D transposed convolutions to generate synthetic infrared thermographic data with three-dimensional spatial structure. The *D* distinguishes between real and generated samples, and the *G* continuously updates its parameters based on the *D* feedback. This iterative adversarial optimization process allows the *G* to produce 3D data whose statistical and spatial characteristics increasingly approximate those of real data. As a result, the input noise vector is progressively transformed into high-quality, physically realistic 3D infrared thermographic volumes.

Finally, the data are fed into the trained model, and the three-dimensional infrared thermographic data generated by the model are merged with the original experimental thermographic volumes to construct a more diverse and comprehensive dataset. Given the large number of three-dimensional thermographic samples after merging, direct analysis poses significant challenges associated with high-dimensional data processing. For this reason, the principal component thermography (PCT) [17] is used to downscale the thermographic samples. It can effectively extract the main spatial features, reduce data redundancy, and improve the efficiency and accuracy of subsequent defect identification and characterization. PCT leverages the strengths of principal component analysis in dimensionality reduction and feature extraction for high-dimensional thermographic data. By processing multi-frame thermographic sequences, PCT transforms the original complex spatiotemporal information into a set of representative principal component images, thereby significantly improving the separation of defect signals from background noise.

4. Experimentation

In this section, quantitative detection and analysis of subsurface defects in CFRP specimens were conducted using the proposed 3DGPCT approach. To comprehensively validate the performance of the method, 3DGPCT was systematically compared with several other extraction techniques. For objective evaluation of detection performance across different methods, the CNR [18, 19] was adopted as a quantitative metric, as it has been widely used for data processing and quality assessment in the field of thermography. By calculating the contrast-to-noise differences between typical defect regions and background areas for each method, the superiority of the 3DGPCT approach is quantitatively demonstrated. The specific calculation formula for CNR is as follows:

$$\mathrm{CNR} = \frac{\left| M_{def} - M_{in} \right|}{\sigma_{in}} \tag{4}$$

here, M_{def} and M_{in} represent the mean pixel values of the defect region and the non-defect (background) region in the thermographic image, respectively. While σ_{in} denotes the standard deviation of pixel values in the non-defect region. The CNR quantifies the contrast between defect and non-defect regions. A higher CNR indicates a greater capability of the method to identify defects.

4.1. Dataset Information

The dataset used in this study was prepared from CFRP specimens, with embedded square Teflon inserts of varying sizes and depths to simulate typical subsurface defect characteristics. Specifically, the defects were classified into three sizes and two depths, labeled as I, II, III and IV, V, VI, resulting in a total of six unique combinations. After epoxy resin infiltration, all defects became invisible. The specific locations and distribution of the defects are illustrated in Figure 2.

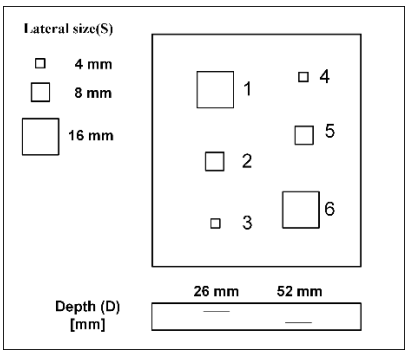

Fig. 2. *Distribution of defects*

During data acquisition, two 3200 W·s flash lamps were first used for thermal excitation. Subsequently, infrared images were captured during the cooling phase using a TAS-G100EXD infrared camera. The acquisition lasted for a total of 2 seconds, recording 60 thermographic images at a resolution of 320×240 pixels. After excluding corrupted frames and retaining only the region of interest for each image, a final dataset of 59 thermographic images with a size of 90×100 pixels

was obtained. Figure 3 shows thermal images at different time points, reflecting the temporal evolution during the acquisition period. As the specimens gradually returned to room temperature, further imaging would not yield additional useful information, resulting in a limited number of thermal images acquired over the brief duration. Moreover, it can be observed that due to significant noise and non-uniform backgrounds in the acquired images, accurate detection and localization of defects are extremely challenging. Therefore, data augmentation is necessary to enrich the diversity of thermographic images and enhance the overall quality of the dataset.

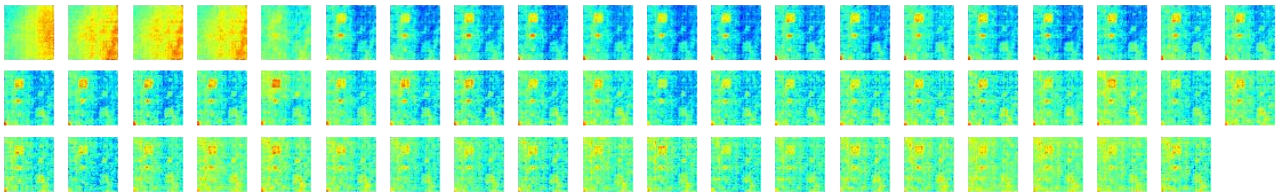

Fig. 3. *Original thermal image*

4.2. 3DGPCT analysis results

After normalization, the data were resized to suitable dimensions and input into the model for training. The model was trained with a learning rate of 0.0001 and a batch size of 7500. Figure 4 shows the thermographic data generated by the trained model. It is noteworthy that the generated images exhibit a global trend highly consistent with the original data. In the early stages, both the original and generated images reflect surface thermal features, and defects are not visible. As time progresses, shallow and deep defects gradually become apparent. In the later stages of acquisition, as the specimen temperature approaches room temperature, the images become dominated by substantial noise.

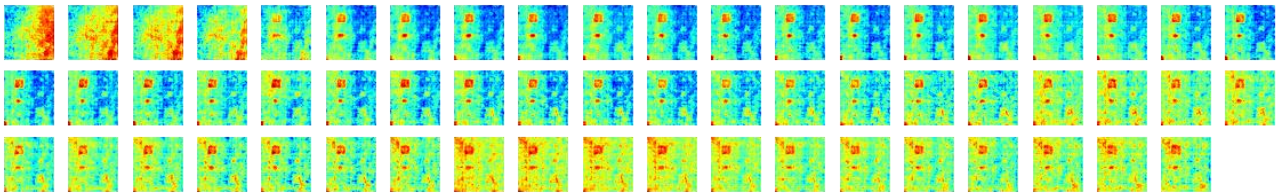

Fig. 4. *Thermal image generated by 3DGPCT*

Subsequently, 15 images were selected from both the acquired and generated datasets to compare the temporal evolution of thermal responses. Overall, the generated images present more distinct defect features compared to the original images, with deep defects also being effectively represented. Notably, defect information remains discernible in the generated images even during the later stages, indicating that the model successfully preserves salient features throughout the learning and training process. During experimental acquisition, as the specimen temperature returns to ambient, the temperature difference between defects and the surrounding material diminishes, causing defect signals to become increasingly obscure. In contrast, the model-generated images are able to alleviate this issue, retaining defect features over a longer temporal span as the temperature equilibrates. The details are shown in Figure 5.

To better observe and localize defects, PCT was applied to the original data, and the first six principal components (PCs) were extracted for analysis and comparison. Similarly, the 3DGPCT model output was also analyzed by extracting its first six PCs. For a comprehensive performance evaluation, conventional GAN and DCGAN models with comparable network architectures were also included for comparison. The images generated by these networks were subjected to PCT, and their first six PCs were analyzed. The visualization results for all four approaches are presented in Figure 6.

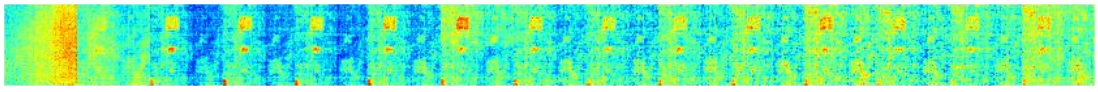

(a) Original image

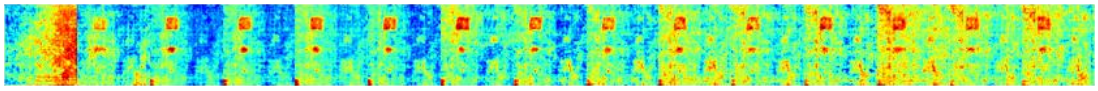

(b) 3DGPCT image

Fig. 5. *Evolution of original image and 3DGPCT image*

In the PCT results of the original images, defects can be faintly detected, but their contrast with the background is limited. In the PCT-processed images generated by the original GAN, shallow defects are distinguishable from the background, whereas deep defects are largely masked by noise. The results from DCGAN are similar, with shallow defects being difficult to observe directly. In contrast, the 3DGPCT model yields highly visible representations of shallow defects and also provides distinct characterization of deep defects. As the specimen temperature returns to equilibrium, fewer of the raw thermographic images visualize deep defects. The 3DGPCT model, however, is able to generate more images

containing deep defect features, thereby enhancing the diversity and richness of the dataset and greatly preserving critical defect information.

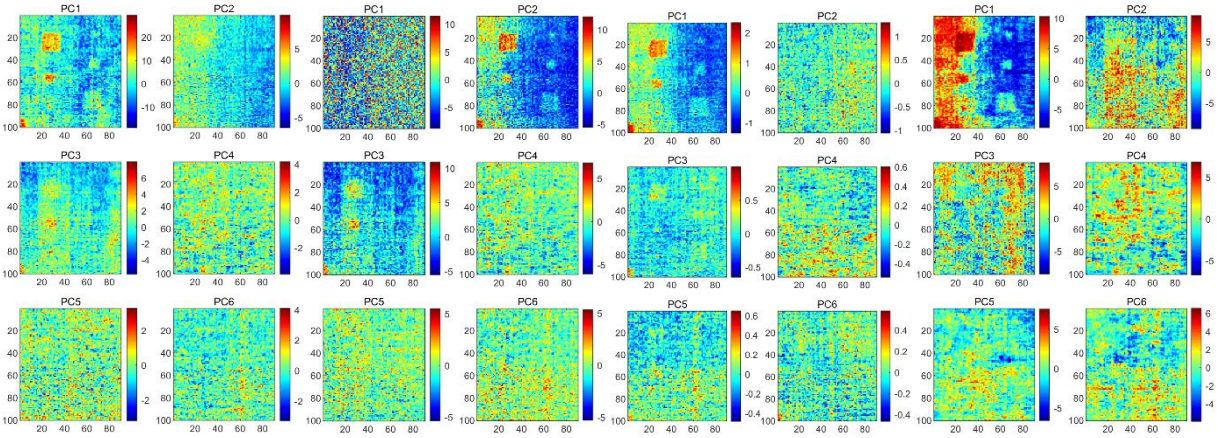

(a) Original (b) GAN (c) DCGAN (d) 3DGAN

Fig. 6. *Results of the four PCT visualizations*

Table 1 presents the quantitative results corresponding to the above visual analyses. It is evident that, for most defect types, the CNR values achieved by the 3DGPCT method are significantly higher than those of the other methods. This indicates that 3DGPCT not only enriches the diversity of the original images but also enhances the representation of defect features, thereby facilitating more accurate defect identification. Furthermore, by incorporating spatiotemporal modeling, 3DGAN is able to more effectively integrate multi-frame or multi-angle feature information, resulting in improved robustness and accuracy in detection. Compared to conventional two-dimensional, 3DGAN demonstrates superior capabilities in capturing and expressing spatiotemporal features, providing richer support for the stereoscopic representation of defect information. Both the visual observations and quantitative metrics such as CNR consistently confirm the outstanding performance of 3DGPCT in defect detection, particularly in expressing spatiotemporal information and accurately identifying deep defects.

Table 1. *CNR results of different methods*

	Defect A	Defect B	Defect C	Defect D	Defect E	Defect F
PCT	2.382	**2.543**	2.084	1.087	0.719	0.809
GAN	2.393	2.363	1.952	0.824	0.725	0.755
DCGAN	1.846	1.706	1.566	0.952	0.614	0.589
3DGAN	**2.432**	2.097	**2.963**	**1.237**	**1.102**	**1.481**

5. Conclusion

In this study, a data augmentation method based on 3DGPCT was proposed and validated for subsurface defect detection in CFRP specimens. By incorporating temporal sequences into the modeling process, the approach effectively mitigates the disappearance of deep defects due to temporal decay. The model not only enriches the diversity of the original thermographic images, but also better preserves the representation of deep defects. The effectiveness of the method was demonstrated on a CFRP sample containing six defects. Comparative experiments with linear and two-dimensional GANs of similar architecture further highlighted the superior performance of the proposed approach. Finally, quantitative evaluation using the CNR metric robustly confirmed the efficacy of the method.

REFERENCES

[1] Gebrehiwet L, Abate E, Negussie Y, et al. Application of composite materials in aerospace & automotive industry[J]. International Journal of Advances in Engineering and Management (IJAEM), 2023, 5(3): 697–723.
[2] Ozturk F, Cobanoglu M, Ece R E. Recent advancements in thermoplastic composite materials in aerospace industry[J]. Journal of Thermoplastic Composite Materials, 2024, 37(9): 3084–3116.
[3] Liu M, Li H, Zhou H, et al. Development of machine learning methods for mechanical problems associated with fibre composite materials: A review[J]. Composites Communications, 2024: 101988.
[4] Zarei A, Pilla S. Laser ultrasonics for nondestructive testing of composite materials and structures: a review[J]. Ultrasonics, 2024, 136: 107163.

[5] Wang Y, Chen Q, Luo Q, et al. Characterizing damage evolution in fiber reinforced composites using in-situ X-ray computed tomography, deep machine learning and digital volume correlation (DVC)[J]. Composites Science and Technology, 2024, 254: 110650.
[6] Hsiao T Y, Sfarra S, Liu Y, et al. Two-dimensional Hilbert-Huang transform-based thermographic data processing for non-destructive material defect detection[J]. Quantitative InfraRed Thermography Journal, 2024: 1–16.
[7] Yagdjian H, Lecompagnon J, Hirsch P, et al. Optimization of thermal shock response spectrum as infrared thermography post-processing methodology using Latin hypercube sampling and analytical thermal N-layer model[J]. Infrared Physics & Technology, 2024, 143: 105582.
[8] Liu Y, Wang F, Liu K, et al. Deep convolutional autoencoder thermography for artwork defect detection[J]. Quantitative InfraRed Thermography Journal, 2024, 21(6): 367–383.
[9] Liu F, Liu J, Wang L. Deep learning and infrared thermography for asphalt pavement crack severity classification[J]. Automation in Construction, 2022, 140: 104383.
[10] Daghigh V, Naraghi M. Machine learning-based defect characterization in anisotropic materials with IR-thermography synthetic data[J]. Composites Science and Technology, 2023, 233: 109882.
[11] Zhang X, Saniie J, Bakhtiari S, et al. Compression of pulsed infrared thermography data with unsupervised learning for nondestructive evaluation of additively manufactured metals[J]. IEEE Access, 2022, 10: 9094–9107.
[12] Guo S S, Lee K H, Chang L, et al. Development of an automated body temperature detection platform for face recognition in cattle with YOLO V3-tiny deep learning and infrared thermal imaging[J]. Applied Sciences, 2022, 12(8): 4036.
[13] Zhao W, Chen F, Huang H, et al. A new steel defect detection algorithm based on deep learning[J]. Computational Intelligence and Neuroscience, 2021, 2021(1): 5592878.
[14] Liu F, Liu J, Wang L. Deep learning and infrared thermography for asphalt pavement crack severity classification[J]. Automation in Construction, 2022, 140: 104383.
[15] Raghavan K, Balasubramanian S, Veezhinathan K. IR-GAN: improved generative adversarial networks for infrared breast image segmentation[J]. Quantitative Infrared Thermography Journal, 2025, 22(1): 70–96.
[16] Cheng L, Tong Z, Xie S, et al. IRT-GAN: A generative adversarial network with a multi-headed fusion strategy for automated defect detection in composites using infrared thermography[J]. Composite Structures, 2022, 290: 115543.
[17] Wang F, Jiang Z, Liu Y, et al. Enhancing defect detection in active infrared thermography using adaptive background suppression techniques[J]. Journal of Thermal Analysis and Calorimetry, 2024: 1–14.
[18] Wang H, Hou Y, He Y, et al. A Physical-constrained decomposition method of infrared thermography: Pseudo restored heat flux approach based on Ensemble Bayesian Variance Tensor Fraction[J]. IEEE Transactions on Industrial Informatics, 2023, 20(3): 3413–3424.
[19] Bu C, Li R, Liu T, et al. Micro-crack defects detection of semiconductor Si-wafers based on Barker code laser infrared thermography[J]. Infrared Physics & Technology, 2022, 123: 104160.